EPJ manuscript No.
(will be inserted by the editor)

Electron-impact dissociation of N_2D^+ cations to D^+ fragments

D.S. Belic[1], M.M. Ristic[2], H. Cherkani-Hassani[3], X. Urbain[4], and P. Defrance[4]

[1] University of Belgrade, Faculty of Physics, PO Box 386, 11000 Belgrade, Serbia
[2] University of Belgrade, Faculty of Physical Chemistry, PO Box 47, 11158 Belgrade, Serbia
[3] Université Sidi Mohamed Ben Abdellah-Fès, Faculté des Sciences Dhar El Mahraz, B.P. 1796, Fès-Atlas 30003, Morocco
[4] Université Catholique de Louvain, Institute of Condensed Matter and Nanosciences, Chemin du Cyclotron 2, B-1348 Louvain-la-Neuve, Belgium

Received: date / Revised version: date

Abstract. Absolute cross sections for electron-impact dissociation of N_2D^+ cations to the light D^+ fragments are reported for the first time. The animated electron-ion crossed-beam method is applied in the energy range from thresholds up to 2 keV. The heavy N_2^+ fragments are also detected and their kinetic energy distribution is analyzed at a selected electron energy. The measured cross-sections are corrected for incomplete collection of the light D^+ fragments by performing careful analyser magnetic field scan together with a Monte-Carlo procedure. Inclusive absolute cross sections are determined. Dissociative excitation (DE) and dissociative ionization (DI) contributions are separated and the corresponding partial cross sections for D^+ fragment production are determined at selected electron energies. The inclusive cross section for D^+ fragment production has a maximum of $(87 \pm 7)\text{x}10^{-18}$ cm^2, at 95.1 eV, with the dominant contribution from the DI process.

PACS. 34.80 Electron and positron scattering – 52.20 Elementary processes in plasmas

1 Introduction

Protonated or deuterated molecular species and their ions are of great importance in plasma chemistry and related phenomena. In particular, they play a role in the low-temperature regions of fusion plasmas [1], in astrophysical phenomena and in the interstellar medium [2]. Such protonated species are also involved in the on-line monitoring of gas impurities at pptv levels by means of proton-transfer-reaction mass spectrometry (PTR-MS), for medical applications, food control and environmental research [3].

The diazenylium cation, N_2H^+, was one of the first ions to be observed in interstellar clouds [4], and has since then been seen in other interstellar environments [5]. It gives information about the fractional ionization and the chemistry that takes place in atmospheric environments, and is often used as a tracer for molecules that are not as easily detected (such as N_2). Its 1-0 rotational transition occurs at 93.174 GHz, a region of the spectrum where the Earth's atmosphere is transparent. It can thus be seen from ground-based observatories. The N_2H^+ ion has been detected in the ionosphere of Titan [6]. This ion is produced mainly via ion-molecule reactions involving the N_2^+, H_3^+, NH^+, H_2^+, N_2 and H_2 species, and thus may provide diagnostics of nitrogen and hydrogen abundances through modeling the complex chemistry of Titan's ionosphere [6].

The neutral N_2H molecule was subject to numerous studies. For both the neutral and the cationic species, non-adiabatic interactions strongly mix their electronic states, which results in a complex electronic spectral pattern. Because of its importance for astrochemistry and atmospheric chemistry, N_2H^+ was widely studied both experimentally and theoretically, and the literature on this cation has been reviewed in detail [7]. The adiabatic three-dimensional potential energy surface (PES) and the corresponding dipole moment surface describing the ground electronic state of N_2H^+ ($X\,^1\Sigma^+$), of linear $C_{\infty v}$ symmetry, have been calculated at different levels of ab initio theory[6],[8]. The ground-state configuration of N_2H^+ is $1\sigma^2\ 2\sigma^2\ 3\sigma^2\ 4\sigma^2\ 5\sigma^2\ 1\pi^4\ {}^1\Sigma^+$. Excitation of either the 5σ or 1π electrons corresponds to the first excited states. It has been pointed out that the lowest-lying excited states of N_2H^+ are mainly dissociating to $N_2^+ + H$ while the first excited state to dissociate into $N_2 + H^+$ is much higher in energy.

Using an *ab initio* methodology, the structure and the electronic excited states of the N_2H^{2+} dication have also been investigated in detail [9]. The ground electronic state of N_2H^{2+} is of $^2\Sigma^+$ term symbol, one in which a 5σ electron is removed from the N_2H^+ ion. Deep potential wells are predicted for this dication in its ground state (0.6 eV below the barrier to the Coulombic repulsive part of the PES leading to the formation of charged fragments) and some of its electronically excited states. There is a dense set of dication excited state potential energy surfaces, that also exhibit a number of avoided crossings arising from degenerate C_s symmetries. These intersections allow for vibronic coupling between states and provide a pathway for fast predissociation. As in isovalent ABH^{2+} triatomic molecular systems, the electronic states of N_2H^{2+} are coupled by vibronic, spin-orbit and Renner-Teller effects. Because of the strong couplings existing in ionic systems between the excited electronic states, the actual dissociation process could involve at least two electronically excited potential surfaces of the molecular ion, thus leading to possible nonadiabatic fragmentation [9].

Most experiments on N_2H^+ are focused on photofragment spectroscopy and ion-molecule reactions [10]. Some dissociative recombination measurements have also been carried out in flowing afterglow [11] and storage ring [12] experiments. After reevaluation of the latter [13], both techniques concluded to a dominant contribution of the N_2 + H channel over the NH + N channel. The yield of electronically excited N_2 molecules from the dissociative recombination of N_2H^+ with electrons has also been studied [14].

Electron impact dissociation and dissociative ionization of the diazenylium cation N_2H^+, more specifically of its isotopologue N_2D^+, have been studied in detail [15]. Absolute cross sections for N_2D^+ fragmentation, producing N_2^+, ND^+, and N^+ heavy-ion fragments, were measured in the 5 to 100 eV range, using a crossed electron beam technique. In that experiment deuterated species was used solely for the purpose of separating the ion fragments produced during dissociation from the parent ion beam. The light D^+ fragment was not detected, neither was the N_2D^{2+} dication, i.e. the product of simple ionization.

Electronic collisions with molecular cations have long been the subject of experimental investigation within our laboratory. By using the animated electron-ion crossed-beam method, diatomic species, such as N_2^+ [16], NO^+ and ND^+ [17],[18], as well as polyatomic, for instance C_2D^+ [19], CD_3^+ [20], O_3^+ [21] were investigated. The diazenylium cation, N_2H^+ has also been studied [22], only regarding dissociation to heavy charged fragments, NH^+ and N^+, in the energy range from reaction threshold up to 2.5 keV.

The production of charged fragments from N_2D^+ due to electron scattering can proceed through various channels, which are listed in [15] and [22]. The following reactions to be considered here are:

$$e^- + N_2D^+ \rightarrow N_2D^{2+} + 2e^- \qquad (SI) \quad (1)$$
$$\rightarrow N_2 + D^+ + e^- \qquad (DE) \quad (2)$$
$$\rightarrow N_2^+ + D + e^- \qquad (DE) \quad (3)$$
$$\rightarrow N^+ + ND + e^- \qquad (DE) \quad (4)$$
$$\rightarrow N + ND^+ + e^- \qquad (DE) \quad (5)$$
$$\rightarrow (N_2D)^* \rightarrow N_2 + D^+ + e^- \qquad (RDE) \quad (6)$$
$$\rightarrow N_2^+ + D^+ + 2e^- \qquad (DI) \quad (7)$$
$$\rightarrow N^+ + ND^+ + 2e^- \qquad (DI) \quad (8)$$

Reaction (1) represents the simple ionization (SI) process. The direct dissociative excitation (DE) processes (2-5) proceed via a vertical transition to either a repulsive excited state or a bound excited state that couples to a dissociative pathway. Both of these pathways result in singly charged fragments. Reaction (2) leads to a light D^+ ion and others give heavy N_2^+, N^+ or ND^+ ions. Three-body fragmentations have not listed here, while their contribution to the various charged products may not be ruled out, specially at the highest collision energies.

The resonant dissociative excitation process (6) proceeds through the resonant capture of an electron to a core excited $(N_2D)^*$ Rydberg state. This state then decays via autoionization and subsequent dissociation, producing charged and neutral fragments. Other dissociative pathways, leading to the same products as (3-5), are also possible. We will refer to both of these processes, direct and indirect, jointly as dissociative excitation (DE).

Dications formed in SI (1) are metastable against dissociation: an electron is removed from the target. Having two positively charged ions initially in close proximity usually leads to two ionic fragments via Coulomb repulsion, completing dissociative ionization processes (7) and (8). In this case, potential energy transfer results in a large increase of the kinetic energy release to the dissociation fragments. The dissociative ionization (DI) processes are in fact in competition with SI and the corresponding signals are time dependent, if the detection occurs in a short period of time after collision. This will be addressed later in the section devoted to the discussion of the results.

One additional process, not considered here, is resonant ion-pair formation (RIP). This proceeds via capture of the incoming electron followed by dissociation at least to two fragments of opposite charge, but the corresponding cross sections for this process are small [15].

Previous experiments [15] and [22] were concerned with heavy ionic fragments production, while the current one will mainly concentrate on the light D^+ fragment. The deuterated target is used and the primary ion beam energy is increased from 8 keV to 12 keV in order to (i) separate neighboring ions, and (ii) to improve the transmission efficiency of the light D^+ fragments from reactions (2), (6) and (7). Inclusive cross sections for the D^+ fragment production are measured in the energy range from threshold up to 2 keV. Measured cross sections are put on an absolute scale by performing scans of the charged fragments with the analyzing magnetic field, associated with a Monte-Carlo simulation. In the same procedure, the DE and DI contributions are determined separately, for selected electron energies. The scans are also used to determine the total kinetic energy released to the fragments.

The experimental procedure is briefly described in the next section. Results are presented and discussed in section 3. First, in subsection 3.1, KER distributions are determined for N_2^+, as they are taken into account in the Monte-Carlo calculation. Subsection 3.2 is devoted to the presentation and discussion of the results obtained for D^+ production.

2 Experimental procedure

The animated crossed electron-ion beam technique is used in this experiment. It has been described elsewhere in detail [23] and only a brief summary is given here. The molecular ion beam is produced in an ECR ion source by introduction of N_2 and D_2 simultaneously. The beam, of 12 keV energy, interacts at right angle with the electron beam of tunable energy, from a few electron volts up to 2 keV. Product ions are separated from the primary ion beam by means of a double focusing 90^o magnetic analyzer. Product ions are further purified and deflected by a 90^o electrostatic spherical deflector to be directed onto a channel electron multiplier.

In the animated electron-ion beam method, the electron beam is swept across the ion beam in a linear motion, at a constant speed u. The total number of events K created during one complete sweep of the electron beam across the ion beam is related to the measured cross section σ_m by the following expression:

$$\sigma_m = \frac{uK}{I_e I_i \gamma} \frac{v_e v_i q_i e^2}{\sqrt{v_e^2 + v_i^2}} \tag{9}$$

Here, γ is the detection efficiency, I_e and I_i, e and q_ie, v_e and v_i, are the electron and ion beam current intensities, the charges and velocities of electrons and ions, respectively.

In the SI process (1) the total signal is detected and the cross section is easily determined by equation (9). In reactions (2-8) the target is first excited to a repulsive intermediate state, from which it spontaneously dissociates. Due to the transfer of internal potential energy into kinetic energy of the fragments, dissociation products exhibit broad angular and velocity distributions in the laboratory frame.

For a particular fragment, the width of the angular distribution θ_M is determined mainly by its maximum kinetic energy of ejection. If θ_M exceeds the angular acceptance of the magnet analyzer $\theta_a = 0.05$ rad, part of the signal is lost. It has been shown [22] that to avoid this loss, the maximum total kinetic energy release (K_M) must satisfy the condition:

$$K_M < \theta_a^2 (E_0 \frac{m_1}{m_2} + V_0) \tag{10}$$

where E_0 is initial kinetic energy of the target, m_1 is the mass of the detected fragment, m_2 is the mass of the residual fragment, and V_0 is the post-collision energy due to application of a positive bias voltage to the collision region.

In the present experiment, E_0=12 keV, V_0=1000 eV, θ_a=0.05 rad and, for the present target (N_2D^+, M=30), application of (10) indicates that the upper limit of K_M is 4.5 eV for the light D^+ fragment.

For DE processes, kinetic energy release distributions (KERD) are usually concentrated in the low energy range, so that the condition (10) is met. However, for DI processes, they may extend up to 15-20 eV due to Coulomb explosion. The particular tests performed here for D^+ showed that full angular acceptance is well achieved for DE, but not for DI. To estimate the loss affecting the DI signal, and hence to determine the DI cross section, a Monte-Carlo simulation may be performed, in combination with a numerical treatment of velocity distributions obtained for N_2^+, the companion of D^+ in the DI process (7).

Fragment velocity distributions, in the laboratory frame, generally exceed the actual magnet transmission window, at a given magnetic field. This results in a further loss of signal which is controlled in the following way [24].

In order to put the cross section on an absolute scale [17], [25], the apparent cross section σ_m(B) is first measured at a given electron energy as a function of the analyzer magnetic field B. Next, the velocity distribution is computed from this cross section scan and the total cross section σ is obtained by integrating this distribution over the entire velocity range. The signal transmission efficiency of the experiment is defined as the ratio of the apparent cross section σ_m(B) and the total cross section σ. This efficiency is used to calculate total absolute cross sections.

Furthermore, the distribution of total kinetic energy released to the dissociation fragments (E_{KER}) is expressed [23] in terms of the above velocity distribution.

The shape of the velocity distribution of the detected fragments depends on the electron energy, i.e. on the various channels involved in the reaction. At low energies, i.e. below the ionization threshold, only DE is observed. The width of the spectrum increases with increasing electron energy, due to the larger kinetic energy released to the fragments associated with the successive opening of possible dissociation channels. Above the ionization threshold, the spectra become even broader as a result of the Coulomb repulsion experienced by the DI fragments. In most cases, DE and DI contributions can be successfully isolated.

In the experimental procedure, analyzer magnetic field scans have been performed at several incident electron energies and transmission factors are extrapolated to the whole considered energy range. They are used (i) to estimate absolute inclusive cross sections, and (ii) to determine separately the absolute DE and DI cross sections.

The total uncertainty is estimated to be about 10% for absolute inclusive dissociation cross sections and, at maximum, to be about 15% for the DE and DI contributions (90% confidence limit). The uncertainty associated with the electron energy is estimated to be $\pm$0.5 eV.

3 Results and discussion

As pointed out in section II, dissociation fragments have broad velocity and angular distributions and this results in a partial loss of signal. This is strongly experienced by the light D^+ fragments and in particular for the DI process.

In order to correct for the loss of D^+ signal, we have used companion N_2^+ fragments from reaction (7), which retain all necessary information, including both fragments DI contributions. The inclusive dissociation cross section

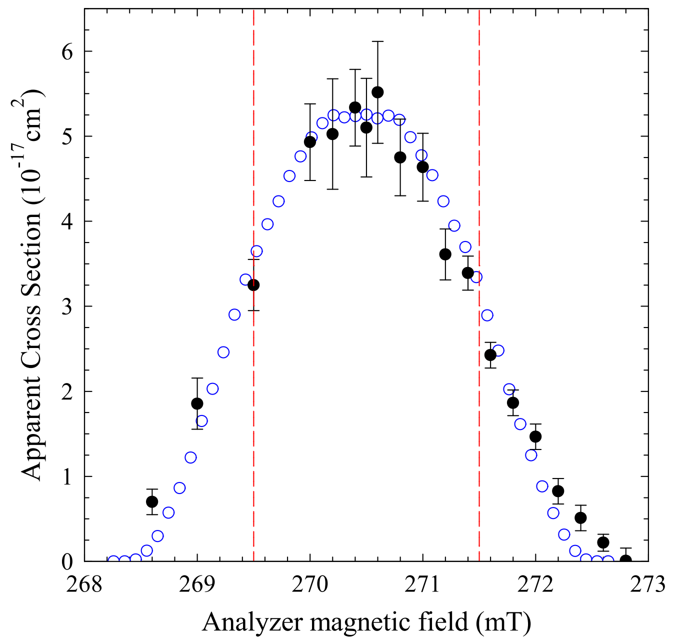

Fig. 1. (Color online) Analyzer magnetic field scan of N_2^+ fragments produced at 95.1 eV. Measured cross sections (solid circles) and Monte Carlo simulations (open circles) are compared. Vertical dashed lines show the acceptance window ΔB (see text).

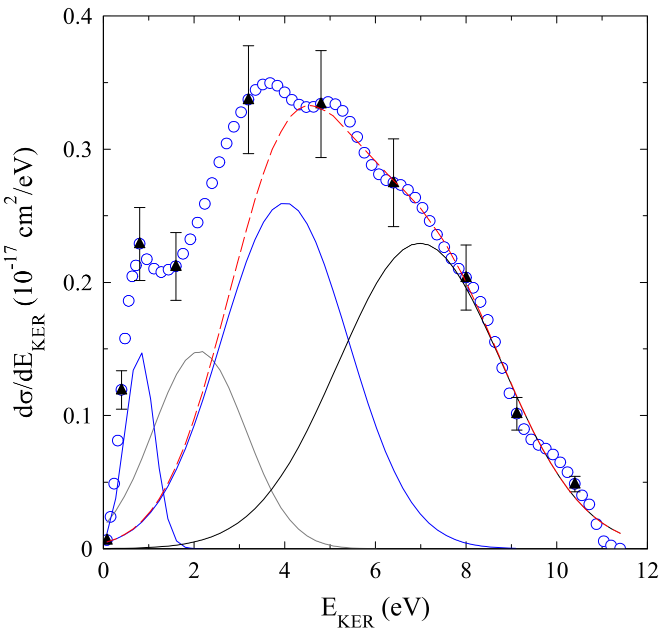

Fig. 2. (Color online) Kinetic energy release distributions of N_2^+ fragments at 95.1 eV: total signal (open circles) is decomposed by four Gaussian contributions (full lines), the sum of which (shown by full triangles) is compared to the total signal. The sum of the two energetic peaks (dashed line) represents total DI contribution.

for N_2^+ heavy ion fragments is determined for the selected electron energy of 95.1 eV. This process is further characterized by performing magnetic field scans of the signal in order to determine the velocity and kinetic energy distributions of the studied fragments.

3.1 Inclusive cross sections and KER distribution for N_2^+ fragment production

In this section we present new results on heavy ion fragment N_2^+ cross section measurements and corresponding kinetic energy distribution. Particular attention is focused on N_2^+ production, since this fragment is partially produced via DI process (7) and thus, by using energy and momentum conservation arguments, brings some valuable information about D^+ fragment production.

The result of the analyser magnetic field scan (σ_m(B)) is presented in Fig.1 for N_2^+ at 95.1 eV. All these heavy fragments enter the analyzer magnet, but only the fraction which corresponds to the interval $\Delta B/B$ equal to 0.007 can be detected at a given magnetic field value [23]. For this particular case, the window ΔB is shown in Fig. 1 by the vertical dashed lines. Thus, the transmission efficiency is determined as the ratio of σ_m(B) integrated over the field window and the integral of the total signal. For this case, at an electron energy of 95.1 eV, the transmission efficiency is found to be 70.5%. In the experiment of Fogle *et al* [15], the transmission efficiency has not been considered and is not included in the data evaluation procedure. El Ghazaly *et al* [22] have not detected N_2^+ fragments, which are very close to the N_2H^+ primary ion beam and thus could not be isolated from the excessive background generated by the latter. The present situation is much more favourable, due to the use of the isotopologue N_2D^+.

The total KER meassured at an electron energy of 95.1 eV for N_2^+ fragment, is shown in Fig. 2. The total kinetic energy of produced fragments is due to reactions (3), (6) and (7) and it is seen to extend up to 11 eV. This distribution has been decomposed by multiple Gaussians fit into four separate contributions, as shown in Fig. 2. The two lower peaks are associated to the direct (3) and resonant (6) DE processes (channel leading to N_2^+ ion), and the two more energetic peaks are believed to be from DI reactions (7). It should be noted here that the latter contributions should be the same as the DI contributions to the production of D^+ fragment via (7). This fact will be used in section III.2 in order to correct for the loss of more energetic D^+ fragments produced by the very same DI process (7).

Here we will bring back our attention to the previous results for absolute cross sections of heavy fragments, N_2^+, ND^+ and N^+, reported by Fogle *et al* [15] and El Ghazaly *et al* [22]. In most cases significant disagreement can be seen between these two sets of data and with the present results. For instance, the total cross section, at 95 eV, derived for N_2^+ fragment by Fogle et al is 4.2x10^{-17} cm^2, and it is found to be (7.2±0.4)x10^{-17} cm^2 from the present experiment.There are two possible explanations for these discrepancies: (i) the transmission efficiency has not been corrected for in the previous data set [15], and (ii) working conditions in [15] or in [22], allow the presence of metastable species in the primary ion beam to be significant and to vary from one case to another. We believe that the first of these two explanations prevails, but the importance of metastable species created in the ion source should not be neglected.

The two previous experimental data sets ([15] and [22]) have been collected from the various thresholds up to 100 eV and 2.5 keV, respectively. Absolute cross sections are determined in a wide energy range, and threshold energies are also determined for each considered fragment. These publications exhibit comparisons of their findings with the existing literature data. In reference [15] comparisons are based on the results of [12] and the NIST data base [26]. These thresholds are extended in [22] by a list of the thermodynamic threshold energies found in the literature. Some of these values for dissociation and ionization are used here, later in analysis of the experimental data on D^+ fragments production.

It has been anticipated [15] that the cross section for "deprotonation" i.e. D^+ formation, would be considerably larger than for the production of other fragments, but this channel could not be measured in the cited experiment. This process will be investigated in the following section.

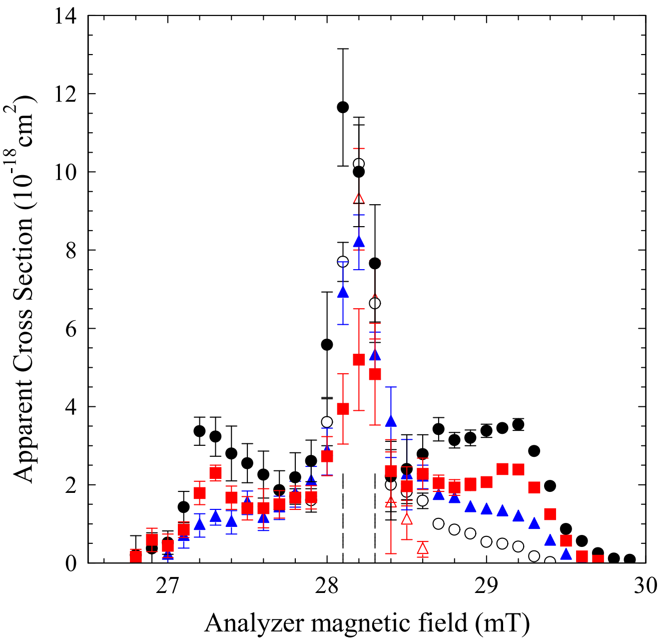

Fig. 3. (Color online) Analyzer magnetic field scans of D^+ produced at electron energies of 19.1 eV (open triangles), 25.1 eV (open circles), 35.1 eV (full triangles), 95.1 eV (full circles) and 295.1 eV (full squares). Dashed lines show the signal transmission window (see text).

3.2 Absolute cross sections for D^+ fragment production

Light D^+ fragments are detected and magnetic field scans of the apparent cross sections are performed at selected electron energies. These results are shown in figure 3, for electron energies of 19.1 eV, 25.1 eV, 35.1 eV, 95.1 eV and 295.1 eV, respectively. Generally, the scans consist of two distinct contributions: the narrower one in the middle is due to the DE contribution and the wider one originates from the DI process. As expected, these scans differ significantly from the above analyzed N_2^+ heavy fragment results (see Fig. 1).

Due to the spread over a relative wider range than the magnetic field window $\Delta B/B$, the average count rate of D^+ is much lower than for instance for N_2^+ fragments. This is one of the reasons why the D^+ fragment was not detected (nor H^+) in the previous experiments [15] and [22].

In particular for high electron energies, the wider part of the spectra, created by the DI process, exhibits a broad dip in the middle. This situation is similar to what was found for D^+ fragments formed by electron impact on ND^+ [18]. In order to minimize this effect in the present experiment we have used the deuterated target N_2D^+, instead of N_2H^+, increasing the mass of the detected fragments. For the same purpose, the kinetic energy of the primary beam was increased from 8 keV [22] to 12 keV, reducing the influence of the kinetic energy release in the centre-of-mass frame on the final velocity distribution of the D^+ fragments in the laboratory frame.

In Fig. 4, the analyzer magnetic field scan of D^+ performed at an electron energy of 95.1 eV, is presented once more to be subjected to further analysis. Apparent cross sections are represented here by solid circles. This spectrum is clearly composed of two contributions. The narrow one in the middle originates mainly from DE process (2). The wider one, from 27 mT to 29.7 mT, with the broad dip in the middle, represents the DI contribution (7). This dip arises from the loss of signal, which is caused by the limited aperture size at the entrance of the magnetic analyzer.

Let us consider the kinematics of the DI process. In the collision region, fragments keep the same velocity in the laboratory frame as the parent ion, but in addition they are sharing the excess of energy liberated, in the centre-of-mass frame, by the dissociation process. The centre magnetic field of the spectrum in Fig. 4 is tuned for the target ion beam velocity. If the dissociation occurs in the centre-of-mass along the beam trajectory, the D^+ fragment may be directed in the forward direction. Its velocity will increase and it will appear at higher magnetic field. On the opposite, when scattered backward, it will acquire a lower velocity and will be detected at lower magnetic field. However, fragments scattered perpendicular to the initial beam velocity will be dispersed in a plane perpendicular to the initial direction. If their divergence exceeds 0.1 radian (full angle) they will hit the entrance aperture and be lost. This situation is experienced by D^+ fragments only, since their mass is much smaller than that of N_2^+ and the velocity they reach in the centre-of-mass frame is significantly higher.

In order to correct our measurements for the loss of signal, we have assumed that the DI signal comes mainly via (7), neglecting possible three body target fragmenta-

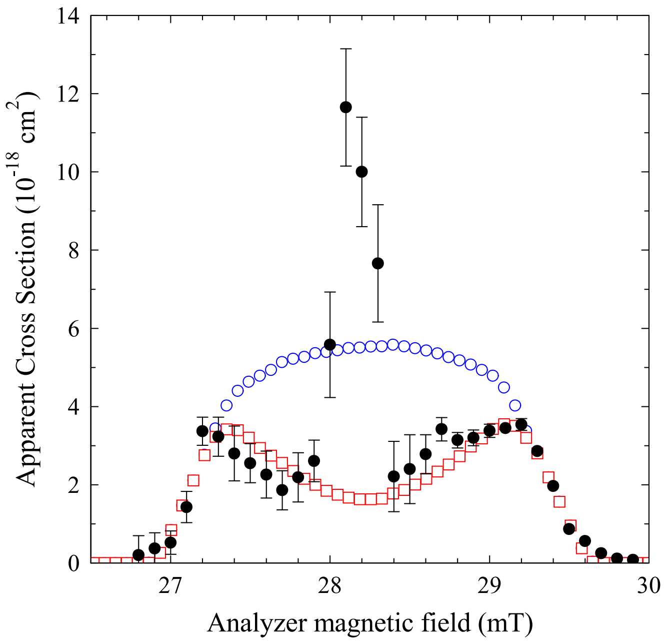

Fig. 4. (Color online) Analyzer magnetic field scan of D^+ fragments produced at an electron energy of 95.1 eV, measured (solid circles), simulated DI contribution (squares) and corrected DI (open circles).

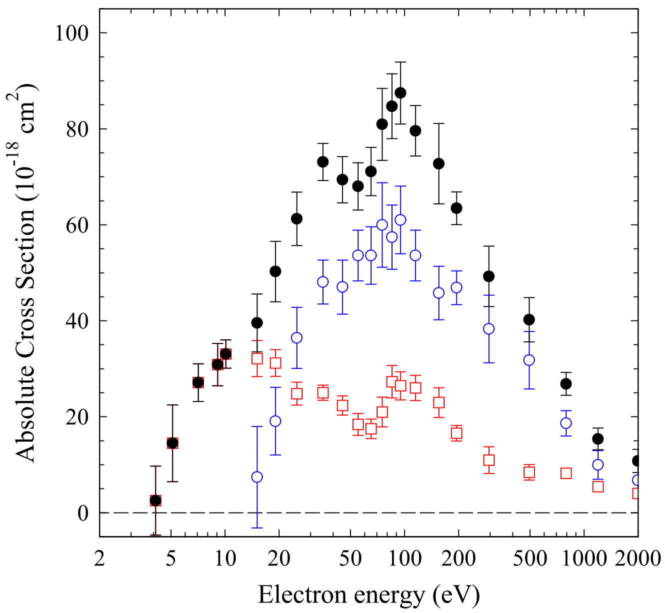

Fig. 5. (Color online) Absolute cross sections for D^+ fragment production by electron impact on N_2D^+ ion: inclusive cross section (solid circles), DE (squares) and DI (open circles).

tion or multiple ionization followed by dissociation. In that case, the DI signal of the D^+ fragment's velocity distribution should be equal to the DI signal contributing to N_2^+ fragments production. Knowing the latter, and employing momentum conservation arguments, it is easy to calculate the D^+ fragments velocity distribution. The velocity distribution of the N_2^+ fragments was already discussed in connection with the N_2^+ magnetic field scan, Fig. 1. The KER distribution of N_2^+ fragment corresponding to DI is shown by the dashed line in Fig. 2.

First, we have tested whether our velocity distribution for N_2^+ is correct. By using the total kinetic energy distribution (Fig. 2) we have applied Monte Carlo simulation to reproduce the magnetic field scan of N_2^+, shown in Fig. 1. The initial velocity of the fragment was selected from the given velocity distribution, by a random number generator. It was used to calculate its trajectory from the collision volume to the entrance of the magnetic analyzer. For a large number of simulated trajectories, the corresponding magnetic field scan may be reconstructed. This signal is normalized at the maximum and the result is shown by open circles in Fig.1. We find the shapes of measured and calculated signal to be in reasonable agreement.

Second, the above described procedure enables us to reproduce the DI contribution of D^+, at an electron energy of 95.1 eV. For this purpose we used the DI velocity distribution for N_2^+, adjusted to D^+ fragments by applying momentum conservation. The result of Monte Carlo simulations is shown with open circles in Fig. 4. The result obtained when taking into account the analyzer magnet entrance aperture, i.e. by eliminating signal with divergence angle greater than 0.1 radian, is shown by open squares in Fig. 4. This result is in a reasonable agreement with the experimental points representing the DI contribution of D^+ (solid circles outside the DE contribution). It turns out that 55.5% of DI signal was lost. In this way, we are able to correct for the loss of D^+ signal at the entrance aperture of the analyzer magnet. The DE contribution, represented by the narrow structure in the middle of the spectrum is 'lifted up' by this DI contribution and this corrected scan is further used to estimate absolute cross section for D^+ fragment production at this energy. The transmission factor is estimated here to be only 14% and absolute cross section at 95.1 eV is found to be $(87\pm7)\text{x}10^{-18}$ cm^2.

Transmission factors for D^+ fragments have been determined for other electron energies at which magnetic field scans were measured. For these energies corresponding transmission factors for DE and DI contributions are determined as well. These results are extrapolated to the complete energy range and the inclusive absolute cross sections for D^+ fragment production are determined. In the same way, corresponding DE and DI cross sections are also determined. They all are presented in Table 1 and are shown in Fig. 5.

The threshold energy for total D^+ cross section is found to be (4.5 ± 0.5) eV. This is in a fairly good agreement with the value of 5.12 eV quoted by El Ghazaly *et al* [22] (among the other thresholds summarized in their table 1). The present value is slightly lower, which is in accordance with the statement of some target ions being vibrationally excited. The cross section maximum is found to be $(87.4\pm6.6)\text{x}10^{-18}$ cm^2, at 95.1 eV. Another, local peak value is seen at 35.1 eV, with the value of $(73.1\pm3.8)\text{x}10^{-18}$ cm^2. This structure results from the two distinct contributions appearing in the DE cross section.

Table 1. Absolute cross sections (in 10^{-18} cm^2) for D^+ fragment production: inclusive (σ_{D+}), DE (σ_{DE}) and DI (σ_{DI}), by electron impact on N_2D^+.

$E(eV)$	σ_{D+}	$\Delta\sigma_{D+}$	σ_{DE}	$\Delta\sigma_{DE}$	σ_{DI}	$\Delta\sigma_{DI}$
4.1	2.5	7.2	2.5	7.2	-	-
5.1	14.5	8.0	14.5	8.0	-	-
7.1	27.1	3.9	27.1	3.9	-	-
9.1	30.8	4.4	30.8	4.4	-	-
10.1	33.1	2.9	33.1	2.9	-	-
15.1	39.5	6.0	32.1	3.7	7.4	10.6
19.1	50.3	6.3	31.2	2.8	19.1	7.0
25.1	61.2	5.5	24.8	2.4	36.4	6.3
35.1	73.1	3.8	25.0	1.6	48.1	4.6
45.1	69.4	4.8	22.4	2.0	47.0	5.6
55.1	67.0	4.9	18.4	2.3	53.6	5.3
65.1	71.1	5.0	17.5	2.0	53.6	5.9
75.1	80.9	7.5	20.9	3.1	59.9	8.8
85.1	84.7	6.7	27.3	3.4	57.4	6.7
95.1	87.4	6.6	26.4	2.9	61.0	7.0
115.1	79.6	5.2	26.0	2.6	53.6	5.3
155.1	72.7	8.4	22.9	3.1	45.8	5.6
195.1	63.4	3.4	16.6	1.6	46.9	3.5
295.1	49.2	6.3	10.9	2.8	38.3	7.0
495.1	40.2	4.6	8.4	1.6	31.8	6.0
795.1	26.8	2.4	8.2	1.1	18.6	2.6
1195.1	15.4	2.3	5.4	0.8	9.9	3.0
1995.1	10.8	2.4	4.0	0.6	6.8	3.5

The threshold energy for the DE contribution is also 4.5 eV, since at low energy, i.e. below the DI threshold, only DE process is present. The DE cross section has a maximum value of (33.1±2.9)x10^{-18} cm^2 at 10.1 eV. This process shows another onset with a threshold energy of 65 eV and has a second local maximum of (27.3±3.4)x10^{-18} cm^2 at 85.1 eV. The DI cross section appears slightly below 20 eV and has a maximum value of (61.0±7.0)x10^{-18} cm^2 at 95.1 eV. The threshold for this process is lower than the value of 20.7 eV, cited in both [15] and [22]. This probably arises from the presence of vibrationally excited species in the primary ion beam. It may be also partly associated to the uncertainty in determining the magnetic field value above which the DE signal disappears from the magnetic field scan and only DI is present.

From the "corrected scan" of D^+ fragments, as discussed above (see Fig. 4), we can draw some conclusions about total KER distribution for the processes leading to D^+ production. However, we are aware of possible uncertainties which can be attributed to the D^+ signal correction procedure and the complexity of the two signals (DE and DI) separation method.

Based on the half width of the central distribution, one deduces a low energy contribution corresponding to DE that extends up to 4 eV, which is in reasonable agreement with the dissociation energies to N_2+D^+, as determined by an early experiment consisting of velocity analyzer and a quadrupole field radio-frequency mass filter [27].

According to the magnetic field scan, the maximum available kinetic energy released to the fragments extends up to 11 eV. This covers the same energy range found for other channels leading to the heavy fragments production, in particular the N_2^+ fragment, as discussed in section III.1.

The kinetic energy released by the Coulomb explosion of the molecule may be estimated from the linear geometry of the ground potential energy surface of N_2D^+. The equilibrium distances have been experimentally determined to be $R_{N-N} = 1.094$ Å, and $R_{N-D} = 1.032$ Å [28]. When considering the N_2^+ + D^+ channel to be accessed through a vertical transition to a pure Coulomb potential, and assuming that the charge is localized at the center-of-mass of either fragment, the KER is inversely proportional to the charge separation

$$d = R_{N-N}/2 + R_{N-D}. \quad (11)$$

The corresponding kinetic energy release is 9.12 eV, fully compatible with the limiting value of 11 eV given above.

Finally, one may question the assumption made throughout the paper that DI into N_2^+ and D^+ fragments is the only outcome of N_2D^{2+} fragmentation, contributing to D^+ production. Ab initio calculations [9] bearing on the first 14 potential energy curves of the dication do not indicate other fragmentation channels than N^+ + ND^+ and N_2^+ + D^+, hence support our assumption. At the highest electron energies however, core electrons may be ejected, leading to multiple ionization and fragmentation, as usually observed in X-ray ionization [29]. Their contribution is however quite difficult to quantify.

To the authors knowledge, there are no other available data for absolute cross section values which could be compared with the present results.

4 Summary and conclusions

Electron-impact ionization and dissociation of N_2D^+ cations are investigated. Absolute cross sections for producing light fragment ions, D^+ are reported, for the first time. The animated electron-ion crossed-beam method is applied in the energy range from the respective thresholds up to 2 keV. The N_2^+, heavy ion fragments are also detected and their kinetic energy distribution is analyzed. Measured cross sections for D^+ production are corrected for incomplete transmission, by performing careful analyzer magnetic field scans, and the total, inclusive, absolute cross sections are determined. Owing to this procedure, dissociative excitation (DE) and dissociative ionization (DI) contributions are separated and corresponding partial cross sections for D^+ fragment production are also determined. The inclusive absolute cross section for D^+ fragment production has a maximum value of (87 ± 7)x10^{-18} cm^2, at an electron energy of 95.1 eV, with the dominant contribution from the DI process.

Acknowledgements

This work was supported by the Fonds de la Recherche Scientifique - FNRS through IISN grant agreement No.

4.4504.10. The authors thank the Belgian State for the grant allocated by Royal Decree for research in the domain of controlled nuclear fusion. D.S.B. is grateful for support from Project No. 171016 from the Ministry of Education, Science and Technological Development of the Republic of Serbia. The authors thank the Forschungszentrum Jülich for lending the ECR ion source as well as all the staff members of the IMCN for their assistance in this experiment.

Authors contributions

All the authors were involved in the preparation of the manuscript. All the authors have read and approved the final manuscript.

References

1. R. K. Janev and D. Reiter. *Phys. Plasmas*, 9:4071, 2002.
2. A. Dalgarno. *In Atomic Processes and Applications.* edited by P. G. Burke and B. L. Moiseiwitch (North-Holland), Amsterdam, pp. 109-132, 1976.
3. W. Lindinger, A. Hansel, and A. Jordan. *Int. J. Mass Spectrometry and Ion Processes*, 173(3):191–241, 1998.
4. B. Turner. *Astrophys. J.*, 193:L83, 1974.
5. J. L. Fox and R. V. Yelle. NASA-CR-200657, 1996. and references therein.
6. V. Brites and M. Hochlaf. *J. Phys. Chem. A*, 113:11107, 2009.
7. F. A. Gianturco, Sanjay Kumar, and F. Schneider. *Chemical Physics*, 211:33–46, 1996.
8. A. Papakondylis. *J. Phys. Chem. A*, 120:9660–6, 2016, DOI: 10.1021/acs.jpca.6b10471.
9. V. Brites and M. Hochlaf. *Chemical Physics Letters*, 477:48–51, 2009, doi:10.1016/j.cplett.2009.06.078.
10. F. A. Gianturco and G. Materzanini. *Eur. Phys. J. D*, 4:321–330, 1998.
11. C. D. Molek, J. L. McLain, V. Poterya, and N. G. Adams. A Remeasurement of the Products for Electron Recombination of N_2H^+ Using a New Technique: No Significant NH + N Production. *The Journal of Physical Chemistry A*, 111(29):6760–6765, 2007. PMID: 17542564.
12. W. D. Geppert, R. Thomas, J. Semaniak, A. Ehlerding, T. J. Millar, F. Österdahl, M. af Ugglas, N. Djurić, A. Paál, and M. Larsson. Dissociative Recombination of N_2H^+: Evidence for Fracture of the NN Bond. *Astrophys. J.*, 609(1):459–464, Jul 2004.
13. E. Vigren, V. Zhaunerchyk, M. Hamberg, M. Kaminska, J. Semaniak, M. af Ugglas, M. Larsson, R. D. Thomas, and W. D. Geppert. *Astrophys. J.*, 757:34, 2012, doi:10.1088/0004-637X/757/1/34.
14. Richard E. Roseti and Rainer Johnsen. *J. Chem. Phys.*, 120:8025, 2004, doi: http://dx.doi.org/10.1063/ 1.1695314.
15. M. Fogle, E. M. Bahati, M. E. Bannister, S.H. M. Deng, C. R. Vane, R. D. Thomas, and V. Zhaunerchyk. *Phys. Rev. A*, 84:032714, 2011, DOI: 10.1103/PhysRevA.84.032714.
16. E. M. Bahati, J. J. Jureta, D. S. Belic, H. Cherkani-Hassani, M. O. Abdellahi, and P. Defrance. *J. Phys. B: At. Mol. Opt. Phys.*, 34:2963–2973, 2001.
17. D. S. Belic, X. Urbain, H. Cherkani-Hassani, and P. Defrance. *J. Phys. B: At. Mol. Opt. Phys.*, 49:135202, 2016.
18. J. Lecointre, D. S. Belic, S. Cherkani-Hassani, and P. Defrance. *Eur. Phys. J. D*, 63(3):441–448, 2011.
19. J. Lecointre, H. Cherkani-Hassani, S. Cherkani-Hassani, Dragoljub S. Belic, Jozo J. Jureta, and P. Defrance. *Eur. Phys. J. D*, 60(2):331–345, 2010.
20. J. Lecointre, D. S. Belic, J. J. Jureta, R. K. Janev, and P.Defrance. *Eur. Phys. J. D*, 55(3):569–580, 2009.
21. D. S. Belic, X. Urbain, and P. Defrance. *Phys. Rev. A*, 91:012703, 2015, DOI: 10.1103/PhysRevA.91.012703.
22. M. O. El Ghazaly, J. B. A. Mitchell, J. J. Jureta, and P. Defrance. *J. Phys. Chem. A*, 118(43):10020, 2014, DOI: 10.1021/jp5084967.
23. J. Lecointre, D. S. Belic, H. Cherkani-Hasani, J. J. Jureta, and P. Defrance. *J. Phys. B: At. Mol. Opt. Phys.*, 39:3275, 2006.
24. Dragoljub S. Belic and Pierre Defrance. *J. Serb. Chem, Soc.*, 65(5-6):439–444, 2000, https://www.researchgate.net/publication/26402974.
25. D. S. Belic, X. Urbain, H. Cherkani-Hasani, and P. Defrance. *Phys. Rev. A*, 95:052702, 2017, DOI: 10.1103/PhysRevA.95.052702.
26. NIST Chemistry WebBook. NIST Standard Reference Database 69, 2011. and references therein.
27. D. Doverspike, R. L. Champion, and T. L. Bailey. *The Journal of Chemical Physics*, 45:4385, 1966.
28. Richard J Saykally, Thomas A Dixon, Thomas G Anderson, Peter G Szanto, and R Claude Woods. Laboratory microwave spectrum and rest frequencies of the N_2H^+ ion. *The Astrophysical Journal*, 205:L101, 1976.
29. R Guillemin, Pietro Decleva, Mauro Stener, C Bomme, T Marin, L Journel, T Marchenko, RK Kushawaha, K Jänkälä, N Trcera, et al. Selecting core-hole localization or delocalization in CS_2 by photofragmentation dynamics. *Nature communications*, 6(1):1–6, 2015.